Inorganic Chemistry

Article

pubs.acs.org/IC

Exchanging Conformations of a Hydroformylation Catalyst Structurally Characterized Using Two-Dimensional Vibrational Spectroscopy

Matthijs R. Panman, Jannie Vos, Vladica Bocokić, Rosalba Bellini, Bas de Bruin, Joost H. N. Reek, and Sander Woutersen*

Van 't Hoff Institute for Molecular Sciences, University of Amsterdam, Science Park 904, 1098 XH Amsterdam, The Netherlands

Supporting Information

ABSTRACT: Catalytic transition-metal complexes often occur in several conformations that exchange rapidly (<ms) in solution so that their spatial structures are difficult to characterize with conventional methods. Here, we determine specific bond angles in the two rapidly exchanging solution conformations of the hydroformylation catalyst (xantphos)Rh(CO)$_2$H using two-dimensional vibrational spectroscopy, a method that can be applied to any catalyst provided that the exchange between its conformers occurs on a time scale of a few picoseconds or slower. We find that, in one of the conformations, the OC−Rh−CO angle deviates significantly from the canonical value in a trigonal-bipyramidal structure. On the basis of complementary density functional calculations, we ascribe this effect to attractive van der Waals interaction between the CO and the xantphos ligand.

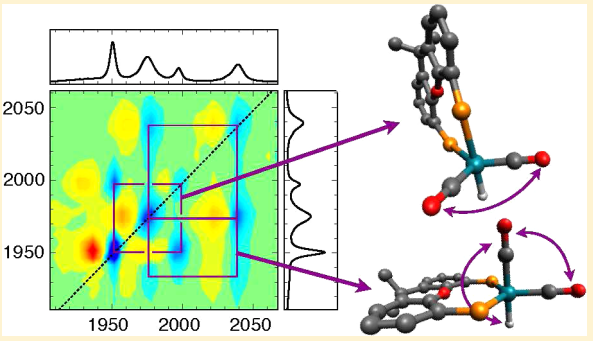

INTRODUCTION

Many catalytic transition-metal complexes exist in several conformations that exchange rapidly (on the ms time scale or faster) under ambient conditions. Generally, these conformations have very different catalytic activities.[1] Hence, to obtain an understanding of how a fluxional transition-metal complex catalyzes a reaction, one ideally would like to characterize all of its conformations in detail. It is, however, very difficult to investigate such rapidly exchanging conformers with conventional experimental methods. X-ray crystallography generally provides access to only a single conformer. The standard method to probe conformations in solution is nuclear magnetic resonance (NMR). However, if the exchange between the conformations is faster than the NMR time scale (determined by the difference between the resonance frequencies of the exchanging conformers, and typically 1 ms),[2] the observed spectrum is an average of the spectra of the different conformers, and the structural information about the individual conformations is lost.

In the infrared (IR) spectrum, the difference between the resonance frequencies is much larger than that in the NMR spectrum. The difference between the CO-stretching frequencies of different conformers of a transition-metal complex is typically several cm^{-1} (10^{11}−10^{12} Hz), which corresponds to a time scale of a few picoseconds. Hence, any exchange taking place more slowly than this time scale is not averaged out in the IR spectrum,[3−7] and the exchanging conformers appear as well-separated peaks or sets of peaks. IR spectroscopy is thus an excellent tool for studying catalytic reactions,[2,8−17] but the conformational information provided by a conventional IR spectrum is rather limited. This limitation can be overcome by using two-dimensional infrared (2D-IR) spectroscopy experiments,[18−21] the IR analog of 2D-NMR spectroscopy. In the pump−probe version of these experiments, one specifically excites a normal mode of a molecule (more precisely, one induces a transition between the v = 0 and v = 1 eigenstates of the molecule−bath system[22]), and by probing the response of all other normal modes, observes the couplings between the excited and the probed modes as cross-peaks in a 2D plot, in a similar manner as in 2D-NMR (COSY). The 2D-IR cross-peak intensities and polarization dependences provide direct information about the relative distance and orientation of the coupled vibrating bonds,[18] information that generally cannot be obtained from the conventional (1D) IR spectrum. Because of its picosecond time resolution, 2D-IR is a powerful method to investigate the structure and dynamics of catalytic transition-metal complexes in solution.[7,19,21,23−29]

Here, we use 2D-IR spectroscopy to study the catalyst (xantphos)Rh(CO)$_2$H (Figure 1, right), a prototypical member of a large class of rhodium catalysts used for the hydroformylation of terminal alkenes.[1,30,31] These catalysts occur in two conformations, one in which the two P atoms are equatorial and the CO ligands are equatorial and axial (here

Received: September 4, 2013

   dx.doi.org/10.1021/ic402254q | Inorg. Chem. XXXX, XXX, XXX−XXX

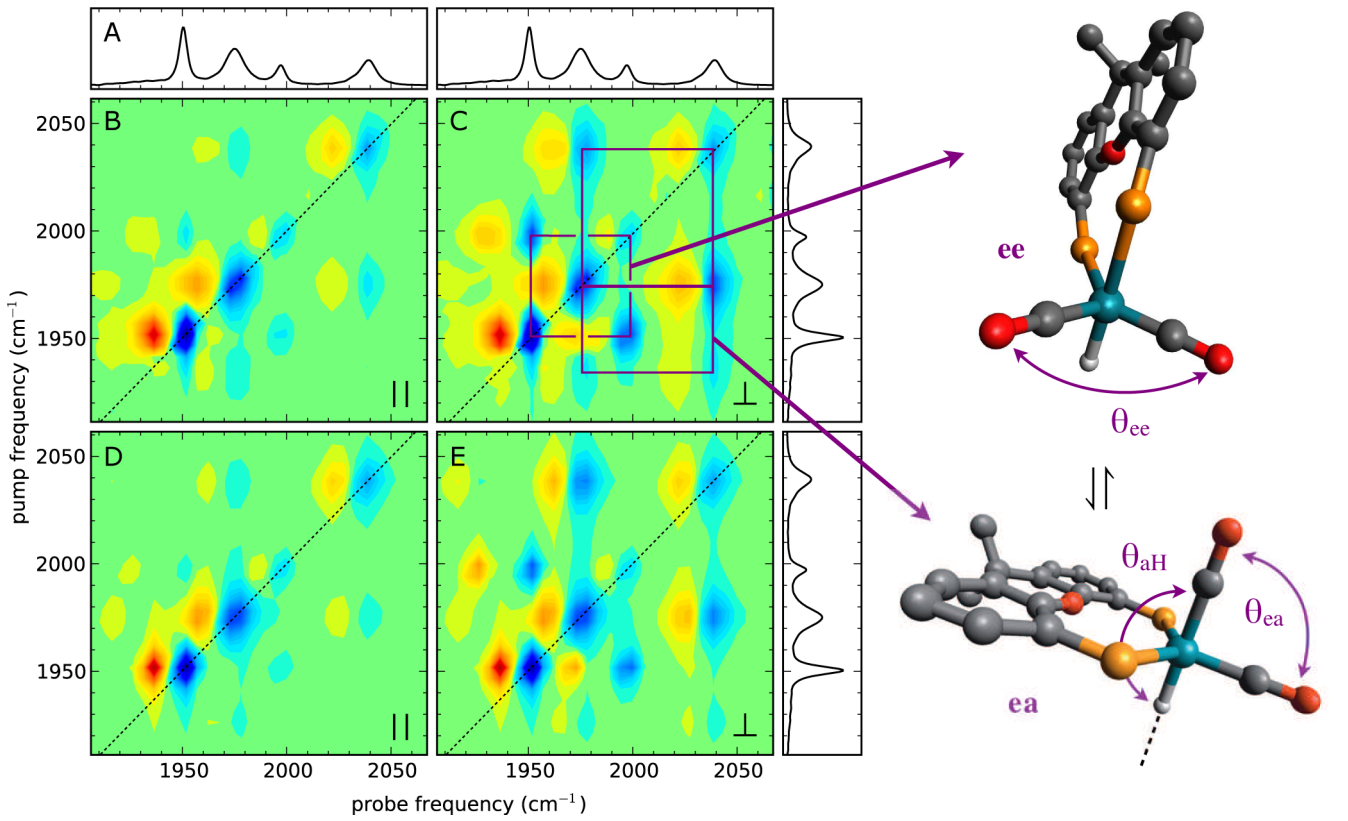

Figure 1. Right: Schematic representation of the two conformers of (xantphos)Rh(CO)$_2$H. The phenyl groups on the P atoms and all H atoms, except the one coordinated to Rh, have been omitted for clarity. (A) Conventional IR absorption spectrum of (xantphos)Rh(CO)$_2$H. The labels "e" and "a" refer to the equatorial and axial positions of the CO ligands. This spectrum is also shown above 2D spectrum C and to the right of 2D spectra C and E. (B, C) 2D-IR spectra of (xantphos)Rh(CO)$_2$H in hexane at 50 bar syngas pressure, for parallel (B) and perpendicular (C) polarizations of the pump and probe pulses, recorded at a delay of 1.8 ps. Red colors denote $\Delta A > 0$, blue colors $\Delta A > 0$, green $\Delta A = 0$. (D, E) Calculated 2D-IR spectra obtained from a global least-squares fit, for parallel (D) and perpendicular (E) polarizations of the pump and probe pulses, using $\theta_{ee} = 121°$, $\theta_{ea} = 108°$, and $\theta_{aH} = 170°$, as obtained from a global least-squares fit to the data.

denoted as "ea"), and one in which one P atom is equatorial and the other axial, and the CO ligands are both equatorial (denoted as "ee") (Figure 1, right). These conformers exchange on a 250 ns time scale (estimated by extrapolating low-temperature NMR data; see the Supporting Information), so in the IR spectrum, the two conformers are separately visible. We find that, from the 2D-IR spectrum, we can determine specific bond angles in both the exchanging conformers.

EXPERIMENTAL SECTION

Sample Preparation. The preparation of the (xantphos)Rh(CO)$_2$H sample is based on the procedure described by van der Veen et al.[32] All chemicals were purchased from Sigma Aldrich and were used without further purification. We dissolved 3.87 mg (1.5×10^{-5} mol) of (acetylacetonato)dicarbonylrhodium(I) in 5 mL of degassed cyclohexane under an inert atmosphere (Ar). A separate solution of 34.72 mg (6.0×10^{-5} mol) of 4,5-bis(diphenylphosphino)-9,9-dimethylxanthene (xantphos) in 25 mL of degassed cyclohexane under an inert atmosphere was prepared in a home-built in situ infrared autoclave. The autoclave was heated to 60 °C and pressurized to 50 bar with syngas under continuous stirring. The formation of the (xantphos)Rh(CO)$_2$H complex was followed with FTIR after the high-presssure injection of the (acetylacetonato)dicarbonylrhodium(I) solution into the xantphos mixture. A portion of the mixture was transferred, under pressure, to a modified high-pressure IR cell (HPL-C-13, Harrick Scientific). The sample was kept between two CaF_2 windows separated by a 1 mm spacer.

Two-Dimensional Infrared Spectroscopy Setup. Using an experimental setup that has been described previously,[33] we generate mid-infrared pulses with a duration of ~100 fs at 2000 cm^{-1} and an energy and bandwidth of 10 μJ and ~200 cm^{-1}, respectively. Probe and reference pulses are obtained from the mid-IR by reflection off the front and back surfaces of a wedged BaF_2 window. Each beam is approximately 5% of the total intensity of the mid-IR radiation. The remainder of the light is used as a pump beam. Both the probe and the reference beams are focused through the sample by means of an f = 100 mm off-axis parabolic mirror. The probe is 200 μm in diameter at the sample. The mid-IR reference beam passes through an area of the sample not influenced by the pump (the purpose of the reference beam is to correct for small pulse-to-pulse fluctuations in the infrared intensity). The changes induced in the sample by the pump pulse are monitored by the mid-IR probe pulses, at various time delays between the pump and mid-IR probe pulse. The delay between pump and probe pulses is controlled with a motorized delay stage. The beams are recollimated with a second f = 100 mm off-axis parabolic mirror. The probe and reference are focused into a spectrograph (MS260i, Newport Oriel) by a third f = 100 mm off-axis parabolic mirror. The spectrograph images both beams onto a 2 × 32 pixel HgCdTe array detector (MCT, Infrared Associates). The pump pulses are optically filtered using a Fabry–Perot interferometer. This results in spectrally narrow pump pulses with a bandwidth of 10 cm^{-1} and an energy of approximately 1 μJ. The center frequency of the light is varied by adjusting the distance between the parallel mirrors of the Fabry–Perot filter using a feedback-controlled piezoelectric mount. To provide the feedback, we project the pump beam after it has passed the sample onto the probe array of the MCT detector. We achieve this by overlapping pump and probe on an adjustable CaF_2 plate that then couples the pump into the spectrograph. Since pump and probe now run collinearly from the plate onward, a bipositional flag is placed such

dx.doi.org/10.1021/ic402254q | Inorg. Chem. XXXX, XXX, XXX–XXX

that it blocks the probe and reference during the optimization of the Fabry–Perot etalon and the pump when data are acquired for the measurement. The delay between pump and probe pulses is controlled with a motorized delay stage. The pump is optically chopped at half the laser repetition frequency to provide the pumped and unpumped shots necessary for the generation of the difference absorption spectrum. The pump pulses have an intensity envelope that is an approximately single-sided exponential with a fwhm of 800 fs, as determined from a cross-correlation measured using two-photon absorption in InAs. The polarization of the IR pump pulse is set at 45° with respect to that of the probe pulse using a MgF_2 zero-order $\lambda/2$ plate. Subsequently, the polarization of the measured spectrum is selected using a rotating polarizer situated directly after the sample set at either 0° (parallel spectrum) or 90° (perpendicular spectrum) with respect to the pump polarization.

RESULTS AND DISCUSSION

Figure 1A shows the IR spectrum of (xantphos)Rh$(CO)_2$H in hexane at 50 bar syngas pressure. The spectrum consists of four intense peaks at 1950, 1975, 1997, and 2040 cm^{-1}, and a weaker shoulder at ~1930 cm^{-1}. We expect five peaks in total for the two conformers: two CO-stretch modes (symmetric and antisymmetric) for the ee conformer, and three CO/Rh–H combinations for the ea conformer. The Rh–H mode contributes to the spectrum only in the ea conformer, because this mode gains sufficient absorption intensity to be observable only if it mixes with the CO-stretch modes (the intrinsic absorption of the Rh–H-stretch mode is much smaller than that of the CO-stretch modes[32]), and the Rh–H/CO mixing is much stronger in the ea conformer than in the ee conformer, since in the former one of the CO bonds is parallel to the Rh–H bond. From the conventional IR spectrum, it is only possible to determine which of the five peaks belong to which conformer by means of isotope labeling,[34] but this question can be solved directly by inspection of the 2D-IR spectrum, shown in Figure 1B,C for parallel (B) and perpendicular (C) polarizations of the pump and probe pulses. In this 2D graph, the absorption change ΔA is plotted as a function of the pump and probe frequencies. On the diagonal, we observe four positive–negative couplets when ν_{pump} is resonant with one of the four most intense absorption bands. The negative ΔA feature is due to the $\nu = 0 \rightarrow 1$ bleaching and $\nu = 1 \rightarrow 0$ stimulated emission of the excited vibrational mode, and the positive ΔA feature is due to $\nu = 1 \rightarrow 2$ excited-state absorption, which is decreased in frequency with respect to the $\nu = 0 \rightarrow 1$ frequency as a consequence of the anharmonicity of the CO-stretch potential. The diagonal peak of the lowest-frequency mode is too weak to be observable. Coupling between vibrational modes causes cross-peaks in the 2D-IR spectrum. Like the peaks on the diagonal, these cross-peaks are also positive–negative doublets. This can be understood as follows. When two modes A and B (with $\nu = 0 \rightarrow 1$ frequencies ν_A and ν_B) are coupled, the frequency of the state in which both modes are in the $\nu = 1$ state is $< \nu_A + \nu_B$ by an amount x_{AB} (the cross-anharmonicity), which is determined by the strength of the interaction between modes A and B.[18] As a consequence, exciting mode A to the $\nu = 1$ state effectively gives rise to a change of $-x_{AB}$ in the $\nu = 0 \rightarrow 1$ frequency of mode B, leading to a negative ΔA at $\nu_{probe} = \nu_B$ and a positive ΔA at $\nu_{probe} = \nu_B - x_{AB}$. The frequency shift x_{AB} is often smaller than the line width, resulting in a cross-peak ΔA signal that (in the ν_{probe} direction) looks approximately like the derivative of the absorption band. In the 2D-IR spectrum of (xantphos)Rh-$(CO)_2$H, cross-peaks are observed between the 1950 and 1997 cm^{-1} modes, and between the 1930, 1975, and 2040 cm^{-1} modes. Since coupling occurs only within a conformer, we can conclude from the cross-peaks that the peak sets {1950, 1997 cm^{-1}} and {1930, 1975, 2040 cm^{-1}} each belong to one of the two conformers. Since the ea conformer should have three peaks, we also can assign the peak sets in the IR spectrum to specific conformations: the {1930, 1975, 2040 cm^{-1}} peaks arise from the ea conformer, the {1950, 1997 cm^{-1} } peaks from the ee conformer. The larger line widths of the ea conformer are probably caused by the contribution of Rh–H stretching in the (mixed C═O + Rh–H stretch) normal modes.

We can use the 2D-IR spectrum to characterize the structure of both the conformers, in particular, to determine the OC–Rh–CO and OC–Rh–H angles θ_{ee}, θ_{ea}, and θ_{aH} defined in Figure 1. These angles determine the dependence of the cross-peak intensities on the angle between the pump and probe polarizations[18] (the contributions of rotational diffusion, fluxionality,[19] and energy transfer[18] to the cross-peak are negligible at our pump–probe delay of 1.8 ps; see the Supporting Information). To obtain the angles and the coupling strengths from the 2D-IR spectrum, we globally fit an excitonic model[18] to the data (details are given in the Supporting Information). It should be noted that, since the strength of the coupling between the modes is of the same order as the difference between their frequencies, the data cannot be analyzed by reading off the cross-peak intensities and anisotropies directly from the 2D-IR spectrum. If the localized C═O and Rh–H stretching modes are used as the basis set, the Hamiltonians of the two conformers are given by

$$H_{ee}^{(1)} = \begin{pmatrix} \varepsilon_e & \beta_{e,e} \\ \beta_{e,e} & \varepsilon_e \end{pmatrix} \text{ and } H_{ea}^{(1)} = \begin{pmatrix} \varepsilon_H & \beta_{H,e} & \beta_{H,a} \\ \beta_{H,e} & \varepsilon_e & \beta_{e,a} \\ \beta_{H,a} & \beta_{e,a} & \varepsilon_a \end{pmatrix}$$

where ε_i are the stretching frequencies of the Rh–H bond (i = H) and of the axial and equatorial CO bonds (i = a, e), and $\beta_{i,j}$ are the couplings between the stretching modes. The angles between the CO bonds in each conformer (see Figure 1, right) enter the calculation through the transition-dipole moment matrix.[18] These angles, the couplings, and site frequencies in the Hamiltonians, together with the anharmonic shifts (the difference between the $\nu = 0 \rightarrow 1$ and $\nu = 1 \rightarrow 2$ frequencies of a local mode), completely determine the 2D-IR spectrum of each conformer. The experimental 2D-IR spectrum is the sum of the 2D-IR spectra of the ee and ea isomers weighted with their relative abundances.

From the fit (shown in Figure 1D,E), we obtain $\theta_{ee} = 121° \pm 1°$, $\theta_{ea} = 108° \pm 3°$, and $\theta_{aH} = 170° \pm 50°$. The complete list of parameters obtained from the fit is given in the Supporting Information. Comparing the coupling strengths obtained from the fit (see the Supporting Information) to the frequency splittings in the IR spectrum, we find that, in both conformers, the contribution of the couplings to the frequency splittings in the IR spectrum is substantial. In the ee conformer, the local-mode CO-stretch frequencies are identical because of symmetry, and the splitting between the IR bands of this conformer is caused purely by the coupling. Accordingly, the coupling obtained from the 2D spectrum (22.8 ± 0.1 cm^{-1}) is exactly half the frequency splitting in the IR spectrum. In the ea conformer, the local-mode frequencies are all different, and the observed differences in frequency of the three IR bands are

dx.doi.org/10.1021/ic402254q | Inorg. Chem. XXXX, XXX, XXX–XXX

caused partly by the coupling and partly by differences in the local-mode frequencies. It is interesting to note that, in the ee conformer, in which the local-mode frequencies are the same because of symmetry, the angle between the CO ligands might, in principle, still be determined from the conventional IR spectrum, but this is not the case for the ea conformer, for which the number of unknown parameters is too large to derive the bond angles from the 1D-IR spectrum. They can be obtained only from the 2D-IR spectrum.

We find that the OC−Rh−CO angle in the ee conformer is equal to the canonical value of 120°, whereas, in the ea conformer, the OC−Rh−CO angle deviates significantly from the 90° expected for an ideal trigonal-bipyramidal structure. To investigate the origin of this deviation, we performed density functional calculations (see the Supporting Information), which we have used previously to investigate similar Rh and Co catalysts.[35,36] We find that geometry optimizations (DFT, BP86, def2-TZVP) without dispersion corrections (attractive van der Waals forces) produce structures with OC−Rh−CO angles close to 90°, deviating significantly from the measured value of 108°. Optimizations including Grimme's dispersion corrections (disp3; DFT-D) lead to a structure (shown in Figure 2) with a larger OC−Rh−CO angle (101°), which is clearly in better agreement with the 2D-IR measurements. Hence, the large θ_{ea} probably arises from van der Waals attraction between the CO ligands and the xantphos ligand. One might think that the observed widening of the OC−Rh−CO angle could be purely the result of steric repulsion, leading to tilting of the axial CO ligand toward the hydride and away from the second CO ligand. However, such behavior was not reproduced with uncorrected DFT methods, which include repulsive steric interactions but lack attractive dispersion forces. Only upon including Grimme's dispersion corrections (disp3) was a calculated OC−Rh−CO angle of 101° obtained, showing that attractive van der Waals forces cause the deviation of the OC−Rh−CO angle from 90°.

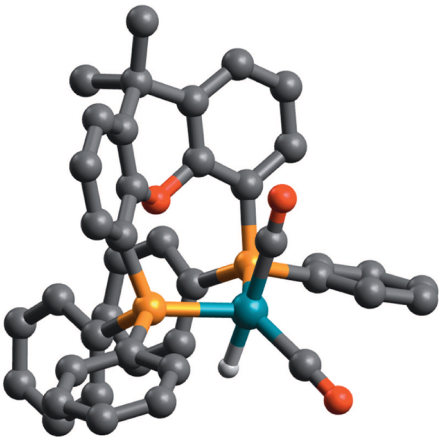

Figure 2. Calculated structure of the ea conformer of (xantphos)Rh-$(CO)_2H$. All H atoms, except the one coordinated to Rh, have been omitted for clarity.

CONCLUSION

To conclude, we have used 2D vibrational spectroscopy to unravel the IR spectrum of a hydroformylation catalyst that occurs in two rapidly exchanging conformations, and to characterize the spatial structure of these conformations. We find that, in one conformer, there exists significant distortion from the ideal trigonal-bipyramidal geometry, probably due to Van der Waals attraction between the CO and xantphos ligands. Such detailed structural information about the conformations of fluxional complexes is difficult to obtain from conventional spectroscopic methods (including 1D-IR spectroscopy). Similar 2D-IR experiments can be performed to determine the exchanging conformations of any fluxional catalyst, provided that the exchange occurs slower than the ∼1 ps time scale corresponding to typical vibrational frequency splittings, and that the bond-stretching modes are at frequencies where subpicosecond IR pulses with sufficient intensity can be generated and detected (∼1000 cm^{-1} and higher). Determination of the coordination geometry of transition-metal complexes in solution is important, as this geometry to a large extent determines their reactivity.[1] In particular, it is well-documented that the bite angle of a bidentate ligand is an important parameter,[37] since ligands with large bite angles lead to relatively unstable square-planar complexes and as such are more reactive than analogues with small bite angles. For hydroformylation, it has been demonstrated that large bite-angle ligands give high selectivity for the linear product. A direct correlation between the relative stability of the resting state and its reactivity in palladium-catalyzed allylic substitution reactions has been reported and used as a basis for a screening protocol.[38] As yet, the crucial information on coordination geometry in catalytic transition-metal complexes is mainly extracted from X-ray analysis of such compounds in the solid state, where packing effects can also play a role. With 2D-IR spectroscopy, we now can obtain such information also for complexes in solution.

ASSOCIATED CONTENT

Supporting Information

Exchange rate of the complex determined from NMR data, delay dependence of the IR pump−probe signals, structural parameters obtained from the global least-squares fit to the 2D-IR spectra, DFT-calculated structures, and corresponding structural parameters. This material is available free of charge via the Internet at http://pubs.acs.org.

AUTHOR INFORMATION

Corresponding Author

*Fax: +31 20 525 6965. Tel: +31 525 7091. E-mail: s.woutersen@uva.nl.

Notes

The authors declare no competing financial interest.

ACKNOWLEDGMENTS

This work was supported by the Stichting voor Fundamenteel Onderzoek der Materie (FOM) and the Nederlandse Organisatie voor Wetenschappelijk Onderzoek (NWO).

REFERENCES

(1) van Leeuwen, P. W. N. M. *Homogeneous Catalysis: Understanding the Art*; Springer: New York, 2004.

(2) Heaton, B., Ed. *Mechanisms in Homogeneous Catalysis: A Spectroscopic Approach*; Wiley-VCH: Weinheim, Germany, 2005.

(3) Harris, C. B.; Shelby, R. M.; Cornelius, P. A. *Chem. Phys. Lett.* **1978**, *57*, 8−14.

(4) Ito, T.; Hamaguchi, T.; Nagino, H.; Yamaguchi, T.; Washington, J.; Kubiak, C. P. *Science* **1997**, *277*, 660−663.

(5) Grevels, F.-W.; Kerpen, K.; Klotzbücher, W. E.; McClung, R. E. D.; Russell, G.; Viotte, M.; Schaffner, K. *J. Am. Chem. Soc.* **1998**, *120*, 10423−10433.
(6) Ito, T.; Imai, N.; Yamaguchi, T.; Hamaguchi, T.; Londergan, C. H.; Kubiak, C. P. *Angew. Chem.* **2004**, *116*, 1400−1405.
(7) Butler, J. M.; George, M. W.; Schoonover, J. R.; Dattelbaum, D. M.; Meyer, T. J. *Coord. Chem. Rev.* **2007**, *251*, 492−514.
(8) To, T. T.; Heilweil, E. J.; Burkey, T. J. *J. Phys. Chem. A* **2006**, *110*, 10669−10673.
(9) To, T. T.; Heilweil, E. J. *J. Phys. Chem. A* **2007**, *111*, 8047−8049.
(10) Sawyer, K. R.; Glascoe, E. A.; Cahoon, J. F.; Schlegel, J. P.; Harris, C. B. *Organometallics* **2008**, *27*, 4370−4379.
(11) Easun, T. L.; Alsindi, W. Z.; Deppermanna, N.; Towrie, M.; Ronayne, K. L.; Sun, X. Z.; Ward, M. D.; George, M. W. *Inorg. Chem.* **2009**, *48*, 8759−8770.
(12) Calladine, J. A.; Torres, O.; Anstey, M.; Ball, G. E.; Bergman, R. G.; Curley, J.; Duckett, S. B.; George, M. W.; Lawes, D. J.; Perutz, R. N.; Sun, X.-Z.; Vollhardt, K. P. C. *Chem. Sci.* **2010**, *1*, 622−630.
(13) Kubis, C.; Ludwig, R.; Sawall, M.; Neymeyr, K.; Börner, A.; Wiese, K.-D.; Hess, D.; Franke, R.; Selent, D. *ChemCatChem* **2010**, *2*, 287−295.
(14) Schneider, J.; Vuong, K. Q.; Calladine, J. A.; Sun, X. Z.; Whitwood, A. C.; George, M. W.; Perutz, R. N. *Inorg. Chem.* **2011**, *50*, 11877−11889.
(15) Lomont, J. P.; Nguyen, S. C.; Zoerb, M. C.; Hill, A.; Schlegel, J. P.; Harris, C. *Organometallics* **2012**, *31*, 3582−3587.
(16) Diebolt, O.; van Leeuwen, P. W. N. M.; Kamer, P. C. J. *ACS Catal.* **2012**, *2*, 2357−2370.
(17) Lomont, J. P.; Nguyen, S. C.; Harris, C. B. *J. Am. Chem. Soc.* **2013**, *135*, 11266−11273.
(18) Hamm, P.; Zanni, M. *Concepts and Methods of 2D Infrared Spectroscopy*; Cambridge University Press: Cambridge, U.K., 2011.
(19) Cahoon, J. F.; Sawyer, K. R.; Schlegel, J. P.; Harris, C. B. *Science* **2008**, *319*, 1820−1823.
(20) Hunt, N. T. *Chem. Soc. Rev.* **2009**, *38*, 1837−1848.
(21) Baiz, C. R.; McRobbie, P. L.; Anna, J. M.; Geta, E.; Kubarych, K. J. *Acc. Chem. Res.* **2009**, *42*, 1395−1404.
(22) Mukamel, S. *Principles of Nonlinear Optical Spectroscopy*; Oxford University Press: Oxford, U.K., 1995.
(23) Golonzka, O.; Khalil, M.; Demirdöven, N.; Tokmakoff, A. *J. Chem. Phys.* **2001**, *115*, 10814−10828.
(24) Bredenbeck, J.; Helbing, J.; Hamm, P. *J. Am. Chem. Soc.* **2004**, *126*, 990−991.
(25) Baiz, C. R.; McCanne, R.; Kubarych, K. J. *Appl. Spectrosc.* **2010**, *64*, 1037−1044.
(26) Stewart, A. I.; Wright, J. A.; Greetham, G. M.; Kaziannis, S.; Santabarbara, S.; Towrie, M.; Parker, A. W.; Pickett, C. J.; Hunt, N. T. *Inorg. Chem.* **2010**, *49*, 9563−9573.
(27) Anna, J. M.; King, J. T.; Kubarych, K. J. *Inorg. Chem.* **2011**, *50*, 9273−9283.
(28) Bingaman, J. L.; Kohnhorst, C. L.; Avan Meter, G. A.; McElroy, B. A.; Rakowski, E. A.; Caplins, B. W.; Gutowski, T. A.; Stromberg, C. J.; Webster, C. E.; Heilweil, E. J. *J. Phys. Chem. A* **2012**, *116*, 7261−7271.
(29) Messmer, A. T.; Lippert, K. M.; Steinwand, S.; Lerch, E. W.; Hof, K.; Ley, D.; Gerbig, D.; Hausmann, H.; Schreiner, P. R.; Bredenbeck, J. *Chem.—Eur. J.* **2012**, *18*, 14989−14995.
(30) Webb, P. B.; Kunene, T. E.; Cole-Hamilton, D. J. *Green Chem.* **2005**, *7*, 373−379.
(31) Franke, R.; Selent, D.; Börner, A. *Chem. Rev.* **2012**, *112*, 5675−5732.
(32) van der Veen, L. A.; Boele, M. D. K.; Bregman, F. R.; Kamer, P. C. J.; van Leeuwen, P. W. N. M.; Goubitz, K.; Fraanje, J.; Schenk, H.; Bo, C. *J. Am. Chem. Soc.* **1998**, *120*, 11616−11626.
(33) Huerta-Viga, A.; Shaw, D. J.; Woutersen, S. *J. Phys. Chem. B* **2010**, *114*, 15212−15220.
(34) Singular-value decomposition of the concentration dependence of the spectrum would not work, since the relative concentrations of the conformers are independent of the (xantphos)Rh(CO)$_2$H concentration.
(35) Patureau, F. W.; de Boer, S.; Kuil, M.; Meeuwissen, J.; Breuil, P.-A. R.; Siegler, M. A.; Spek, A. L.; Sandee, A. J.; de Bruin, B.; Reek, J. N. H. *J. Am. Chem. Soc.* **2009**, *131*, 6683−6685.
(36) Suarez, A. I. O.; Jiang, H.; Zhang, X. P.; de Bruin, B. *Dalton Trans.* **2011**, *40*, 5697−5705.
(37) Birkholz, M.-N.; Freixa, Z.; van Leeuwen, P. W. N. M. *Chem. Soc. Rev.* **2009**, *38*, 1099−1118.
(38) Wassenaar, J.; Jansen, E.; van Zeist, W.-J.; Bickelhaupt, F. M.; Siegler, M. A.; Spek, A. L.; Reek, J. N. H. *Nat. Chem.* **2010**, *2*, 417.